Supplemental Movies, Figures and Tables

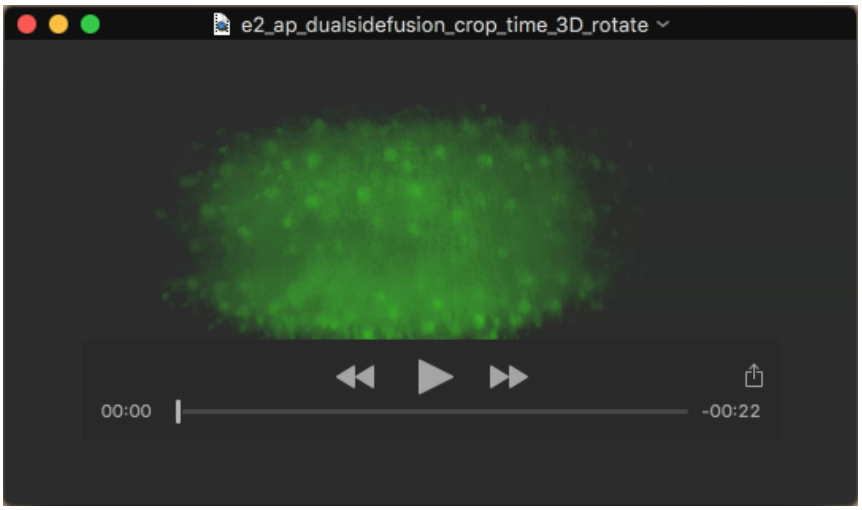

Movie 1 - A Light Sheet time-lapse movie following the dynamics of endogenously expressed Dorsal-GFP in the entire embryo. The nuclear Dorsal gradient, which can be seen in nuclei at the ventral side (bottom) already at NC 12, is lost during nuclear divisions and is re-generated at the onset of each nuclear cycle.

Movie 2 - A frame by frame 2D projection of movie 1 done using the ImSAnE tool (Heemskerk and Streichan, 2015). Dorsal-GFP appears in grey.

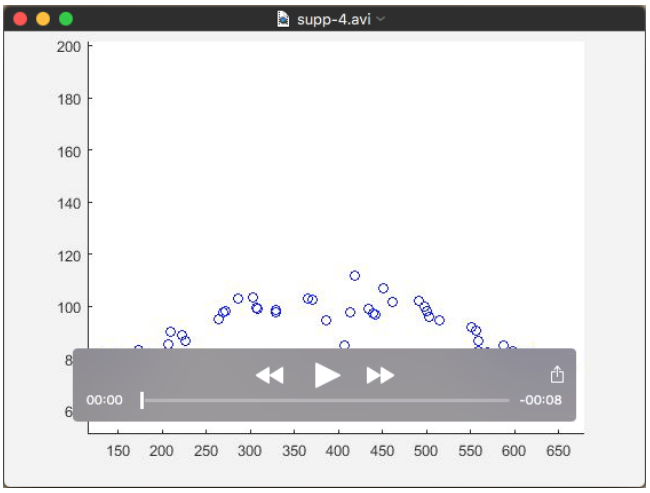

Movie 3 - Time lapse of Dorsal-GFP intensity data for the area inside the dashed frame in Figure 1C. Each circular marker in the movie shows raw, non smoothed Dorsal-GFP intensity in a single nucleus. Nuclei were segmented from the corresponding frames of movie 2 (See Methods).

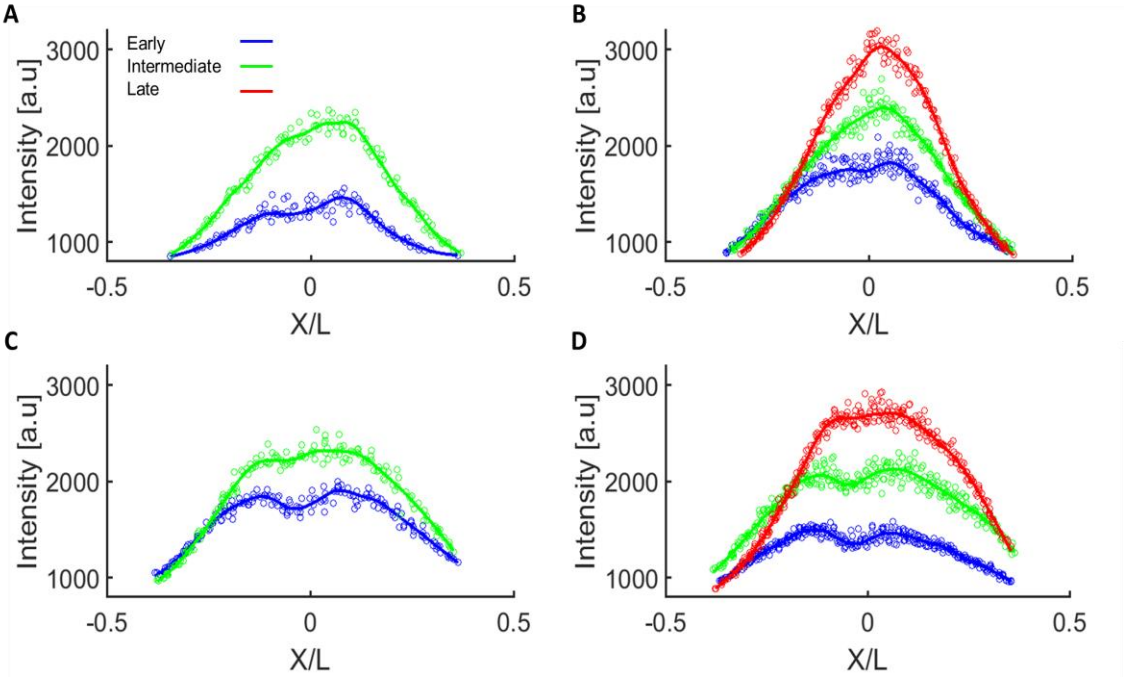

Figure S1- Dorsal temporal dynamics in the embryo- raw and smoothened data. Dorsal-GFP intensity, plotted as a function of relative location along the DV axis for NC 13 (A,C) and NC 14 (B,D) for a *wt* (A,B) and a *wntD*-/- (C,D) embryo. Relative location axis x/L is defined as location divided by embryo circumference (see Methods). For each color coded time point, raw Dorsal-GFP intensity is denoted by the circular markers, and a corresponding smoothened curve is plotted as a solid line of the same color (see Methods). Due to its shorter duration, only two time points are shown for NC 13 (an early time point and the final time point of this cycle).

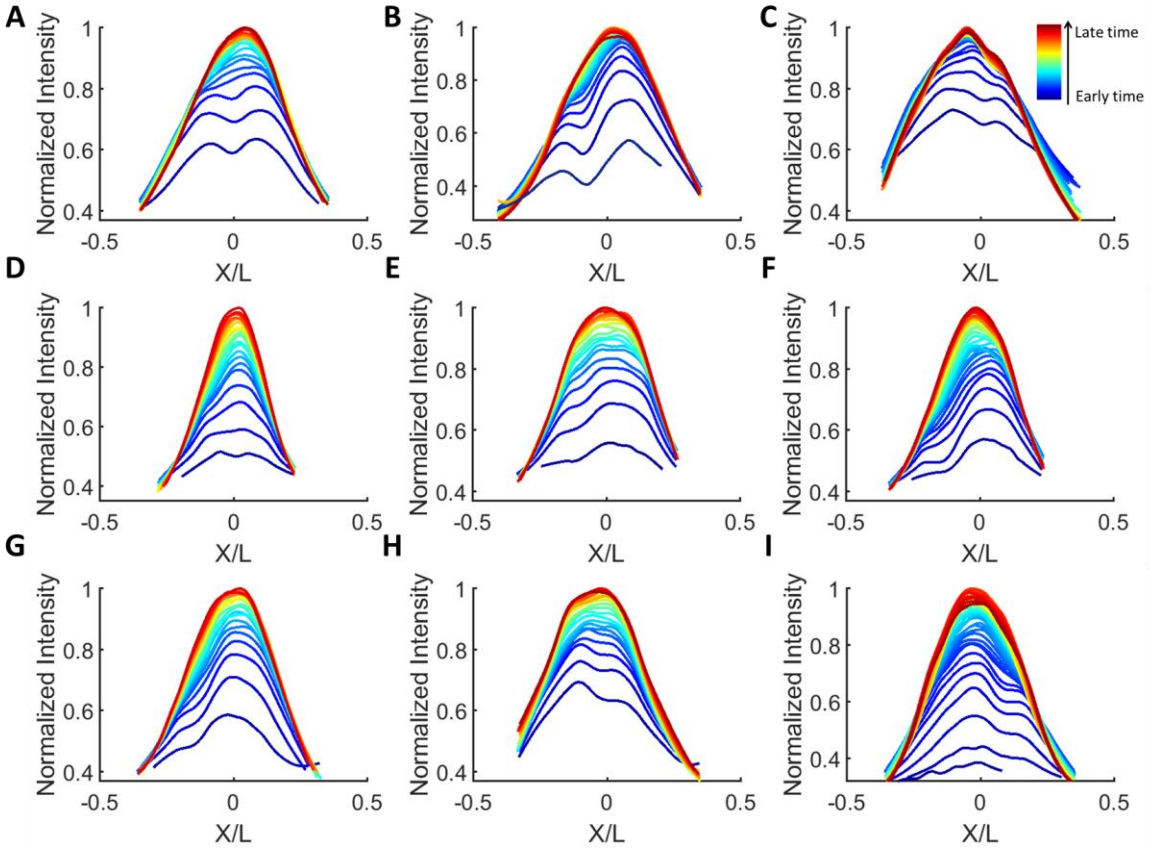

Figure S2 – Dorsal temporal dynamics during NC 14 in *wt* embryos. Dorsal-GFP intensity, plotted as a function of relative location along the DV axis. Relative location axis x/L is defined as location divided by embryo circumference (see Methods). A curve is shown for each time point during NC 14 for 9 *wt* embryos. Each Dorsal-GFP intensity curve was smoothened and normalized by the maximal value attained during NC 14 (see Methods). Time points are 1.5 minutes apart for (A-H) and 1 minute apart for I, ranging from the earliest time points in blue to the latest in red. All embryos exhibit shuttling signatures: lateral overshoots and converging double peaks. The use of Dorsal-GFP may bias the morphogen activity profile due to changes in gene dosage and possible effects of the fusion to GFP. We have also monitored the dynamics in embryos that are heterozygous for endogenous Dorsal, and find qualitatively similar kinetics of Dorsal-GFP nuclear entry. We focus on the dynamic profile of Dorsal-nuclear localization, not on the absolute values which may vary between embryos and between experiments. Thus, while the fusion of Dorsal to GFP may widen its distribution, the two qualitative features of an overshoot and a double peak which are our hallmarks for shuttling, are retained.

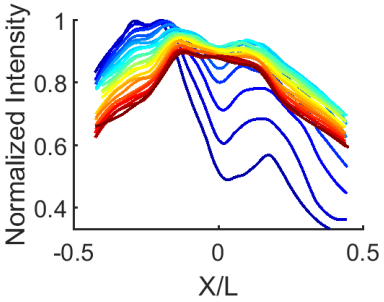

Figure S3 - Shuttling hallmarks are retained in cactus knockdown embryos. Dynamics of Dorsal-nuclear localization in a single *cact* knockdown embryo at nuclear cycle 14 shows a prominent double peak which converges to a flat peak towards the ventral midline. Asymmetry between left and right likely stems from significant tilt of the embryo along the anterior -posterior axis during imaging.

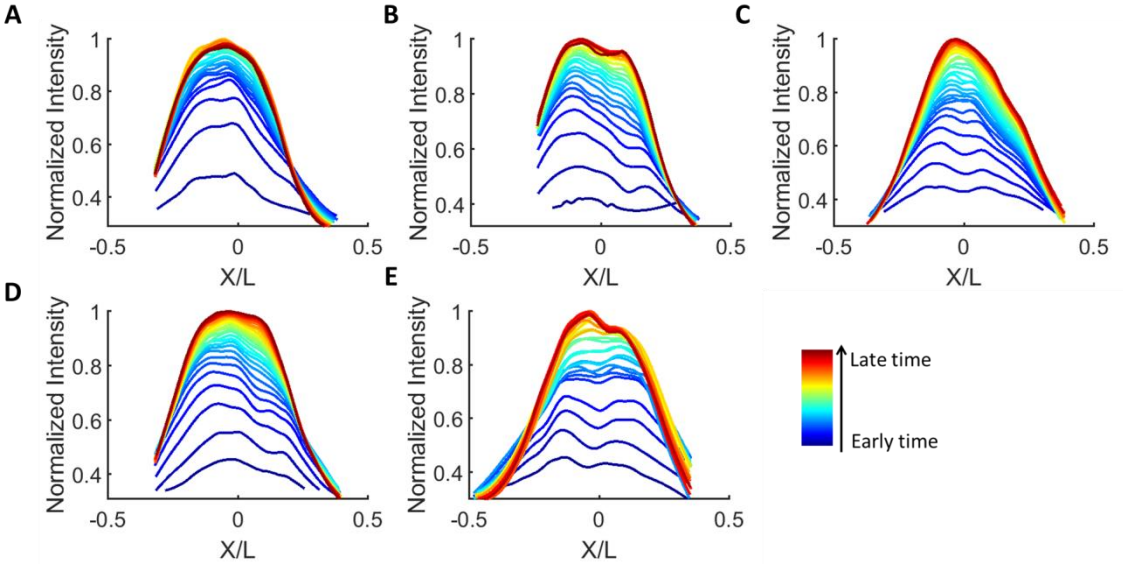

Figure S4 - Dorsal temporal dynamics during NC 14 in *wntD-/-* embryos. Dorsal-GFP intensity, plotted as a function of relative location along the DV axis. Relative location axis x/L is defined as location divided by embryo circumference (see Methods). A curve is shown for each time point during NC14 for 5 *wntD-/-* embryos. Each Dorsal-GFP intensity curve was smoothened and normalized by the maximal value attained during NC14 (See Methods). Time points are 1.5 minutes apart, ranging from the earliest time points in blue to the latest in red. All embryos exhibit shuttling signatures: lateral overshoots and double peaks flattening over time.

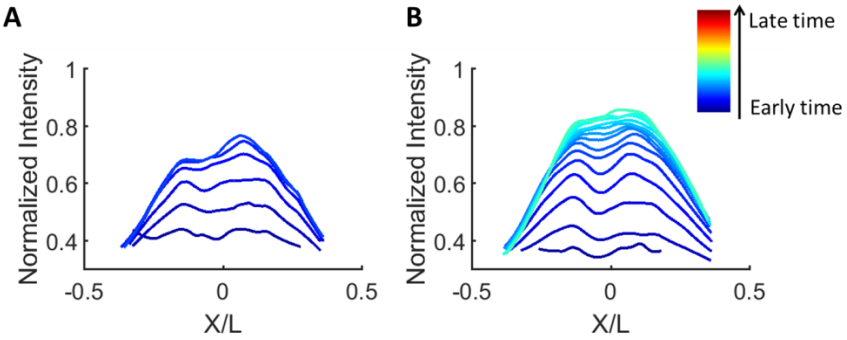

Figure S5 - Dorsal temporal dynamics during NC12-13 in a *wntD-/-* embryo. Dorsal-GFP intensity, plotted as a function of relative location along the DV axis. Relative location axis x/L is defined as location divided by embryo circumference (see Methods). A curve is shown for each time point during NC12 (A) and NC13 (B) for the *wntD-/-* embryo presented in Figure 3E. Each Dorsal-GFP intensity curve was smoothened and normalized by the maximal value attained during NC14 (see Methods, Figure 3E). Time points are 1 minute apart, ranging from earliest time points in blue to the latest in red.

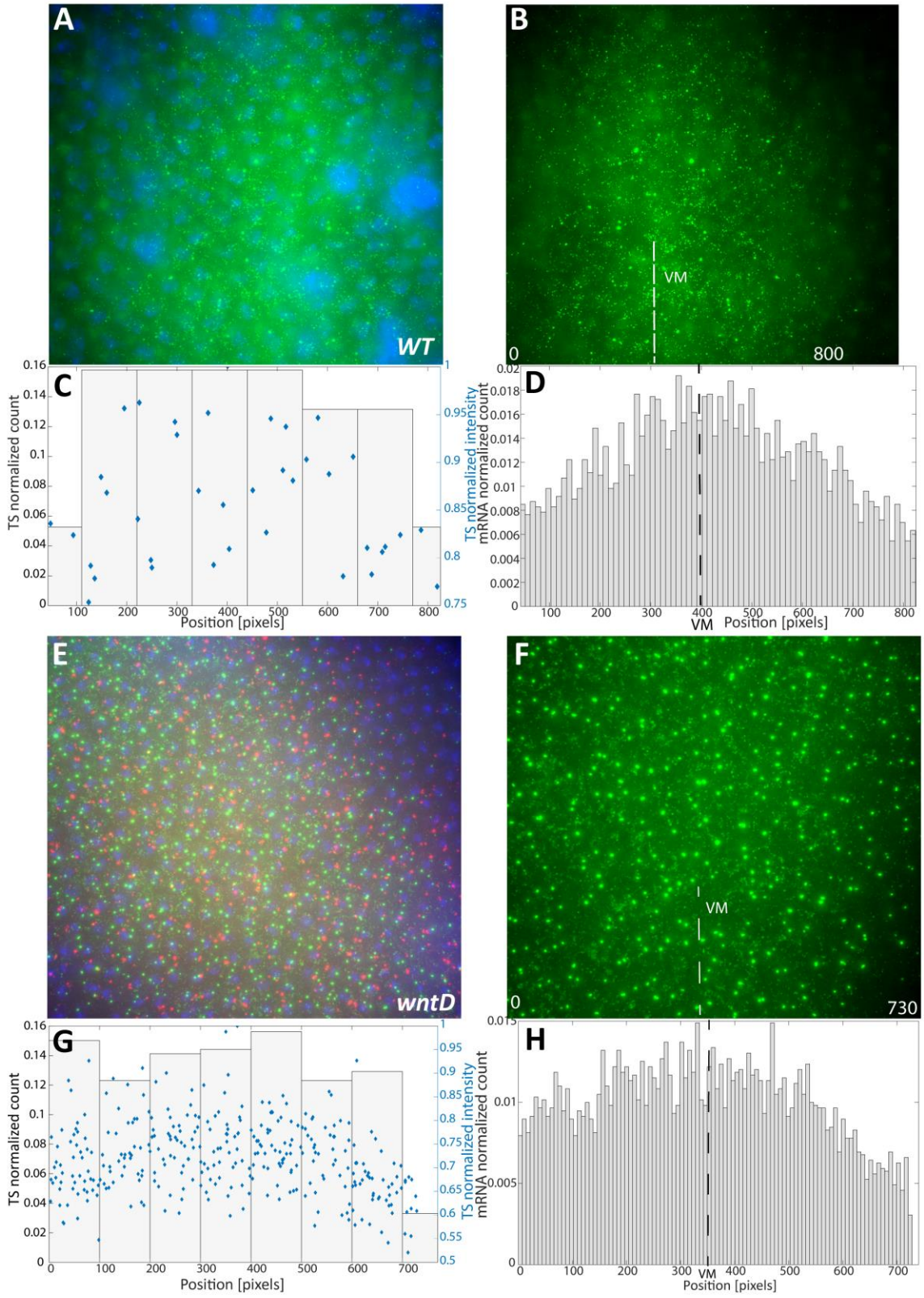

Figure S6 - **Graded accumulation of *T48* transcripts.** (A) Single-molecule FISH with *T48* (green) probes was carried out, to mark the ventral domain of *WT* embryos. We analyzed *T48* signals in embryos that displayed the prominent signals of transcription sites (TS) in nuclei (DAPI-blue) along the entire ventral domain. (B) Magnified and re-oriented view of a portion of the field shown in (A). The position of the ventral midline (VM) is marked. Weaker cytoplasmic signals correspond to individual mature *T48* mRNA molecules. (C) Quantification of the number of TS (displayed as histogram bars) and their intensity (blue dots) at different positions along the D-V axis (0 marks the ventral midline). (D) Quantification of number of weak cytoplasmic *T48* puncta along the D-V axis. The number of mRNA molecules across the ventral domain displays a gradient that peaks at the ventral midline. We thus conclude that while all nuclei are transcribing *T48* at the same rate, the difference in the onset of transcription coupled with the stability of the mRNA, gave rise to a graded distribution of mature transcripts. (E,F) A similar analysis was carried out on *wntD* mutant embryos, at the stage when *T48* and *fog* (red) TS are observed across the ventral domain. (G) The number and intensity of *T48* TS along the ventral domain is constant. (H) In contrast to *WT* embryos, the accumulation of *T48* transcripts is more uniform.

Table S1 : Parameters table for full model, WT values

#	Parameter	Units	Meaning	Value in a.u	Units	Value in units
1	K_{rec}	t^{-1}	Toll receptor recycling rate	0.07	$\sec^{-1}$	0.007
2	K_{end}	t^{-1}	Toll receptor endocytosis rate	1	$\sec^{-1}$	0.1
3	λ	t^{-1}	NCSpz* cleavage rate	4.2	$\sec^{-1}$	0.42
4	α_N	t^{-1}	NSpz degradation rate	0.0011	$\sec^{-1}$	0.00011
5	α_c	t^{-1}	CSpz degradation rate	0.0014	$\sec^{-1}$	0.00014
6	α_{Nc}	t^{-1}	NCSpz degradation rate	0.0016	$\sec^{-1}$	0.00016
7	$K_{on,c}$	$t^{-1}C$	CSpz binding to Toll	0.3	$\mu M\sec^{-1}$	0.0013
8	$K_{off,c}$	$t^{-1}C$	CSpz un-binding from Toll	1.12	$\sec^{-1}$	0.0049
9	K_{on}	$t^{-1}C$	NCSpz binding to Toll	0.008	$\mu M\sec^{-1}$	3.2e-5
10	K_{off}	$t^{-1}C$	NCSpz un-binding from Toll	0.1	$\sec^{-1}$	4.33e-04
11	η_0	$t^{-1}C$	NCSpz activation rate	0.22	$\mu M\sec^{-1}$	9.68e-4
12	K_{bind}	$t^{-1}C$	CSpz binding rate to NSpz	7	$\mu M\sec^{-1}$	0.0308
13	K_{split}	t^{-1}	NCSpz-Tl splitting rate to CSpz-Tl and 2*N-Spz , on Toll	10	$\sec^{-1}$	1
14	D_{NC}	x^2t^{-1}	NCSpz diffusion coefficient	0.1186	$\mu m^2\sec^{-1}$	118.6
15	D_N	x^2t^{-1}	NSpz diffusion coefficient	0.0055	$\mu m^2\sec^{-1}$	55
16	D_{NC*}	x^2t^{-1}	NCSpz* diffusion coefficient	0.745	$\mu m^2\sec^{-1}$	745
17	T_{tot}	C	Total Toll level	5.625	μM	0.25
18	D_W	x^2t^{-1}	WntD diffusion coefficient	0.5	$\mu m^2\sec^{-1}$	500
19	α_w	t^{-1}	WntD degradation rate	0.001	$\sec^{-1}$	1.4e-5
20	β_w	$t^{-1}C$	WntD production rate	0.1	$\mu M\sec^{-1}$	4.4e-4

21	K_w	C^{n_w}	K_D of WntD production as a function of signaling	9e-10	μM^{n_w}	4.7e-30
22	n_w	-	Hill coefficient of WntD production as a function of signaling	15	-	15
23	L	x	Length of tissue	2	μm	250
24	X_{pipe}	%	% of L below which a point $\vec{x} = (x, y, z) \in pipe\ domain$	40	%	40
25	X_{WntD}	%	% of L above which a point $\vec{x} = (x, y, z) \in$ $WntD\ producing\ domain$	25	%	25
26	W_{lower}	%	Maximal lowering of Tl property by WntD	60	%	60
27	W_{Tr}	$C^{n_{lower}}$	K_D of WntD lowering receptor property	5	$\mu M^{n_{lower}}$	0.01
28	n_{lower}	-	Hill coefficient of WntD lowering receptor property	2	-	2
29	T	t	# of discrete time points the simulation was run	600	sec	6000 (~1.5 hours)
30	$K_{Dl,in}$	$t^{-1}C$	Rate of Dl entry into the nucleus	0.07	$\mu M \mathrm{sec}^{-1}$	2.8e-04
31	$K_{Dl,out}$	$t^{-1}C$	Rate of Dl exit from the nucleus	2	$\mu M \mathrm{sec}^{-1}$	0.008
32	Dl_0	C	Initial Dl concentration in the nuclei	1e-4	μM	4.4e-06
33	Dl_{tot}	C	Total amount of Dl	5	μM	0.22

Supplementary Materials and Methods

Mathematical model

Our full model describes how the Spz gradient is formed by shuttling, induces the nuclear localization of Dorsal and the negative feedback between WntD and Dorsal which maintains gradient robustness (Rahimi et al., 2016). To this end, we extend the model from our previous paper (Rahimi et al., 2016) to include the nuclear localization of Dorsal. Also, we used a different mechanism by which WntD contracts the Spz gradient: instead of competing with the ligand for binding the Toll receptor, we assume here that WntD "crowds" the Toll receptor's immediate environment, by binding its own receptor Frizzled-4 and limiting the access of Spz to Toll by physically blocking the receptor. This decreases the chances of ligand binding the receptor and therefore increases the chances of free ligand binding the shuttling molecule, enhancing shuttling. This "crowding" of Toll has an additional affect: stabilizing binding to Toll of the ligand which succeeded in binding the receptor. This effect again depends on WntD bound to Frizzled-4physically blocking the receptor's immediate surroundings and thus blocking ligand from disengaging the receptor. This phenomenon also makes shuttling more efficient, maintaining Toll receptors occupied until they transduce signaling.

The governing set of reaction-diffusion equations of our model is given below. The meaning of the different parameters and their units are summarized in Table S1. This set of equations was solved numerically in 1D using a standard MATLAB PDE solver. **Eqn. 1** defines the temporal dynamics of freely diffusing WntD. The terms of the equation by order of appearance describe: WntD diffusion, WntD degradation, and WntD production, which depends on nuclear Dorsal. This last term is the induction part of InC, as WntD production is positively regulated by signaling. The WntD producing zone is restricted and is defined in the embryo by the Torso signaling border. In the simulations we define this zone using the model parameter X_{WntD}; WntD production is only allowed for points posterior to X_{WntD} . **Eqn. 2** defines the nonlinear saturating function R_w through which WntD changes the properties of the Toll receptor: the rate at which ligands bind and unbind from it. **Eqn. 3** defines the temporal dynamics of free Toll receptors. This equation introduces the following constraint: the total amount of Toll receptors (free, bound by ligand and endocytosed) is constant and equals T_{tot}. **Equations 4-10** are the self-organized shuttling model (SOSH) equations as appear in (Haskel-Ittah et al., 2012). We'll review SOSH and the equations briefly: The SOSH mechanism depends on the versatility of the *Spz* protein. The separate inhibitor domain N-Spz and activating region of *Spz,* C-Spz, generated after cleavage of the NC-Spz precursor (**eqn. 4**), can interact with each other in three different modes. These modes facilitate a process of "self-organized shuttling", where the active ligand C-Spz is shuttled and concentrated at the ventral-most region, giving rise to the sharp activation gradient of *Toll*. Equations 5-7 describe the shuttling of the active C-Spz ligand (which cannot diffuse on its own) by the N-Spz inhibitor when bound together as the NC-Spz* complex. Signaling occurs when C-Spz bound to

Toll undergoes endocytosis (**eqns. 5,8,10**). Toll receptors undergo recycling back to the membrane after endocytosis and the total concentration of Toll is constant (**eqns. 10,3** respectively). The C-Spz ligand and N-Spz inhibitor are products of NC-Spz complex separation when bound to the Toll receptor (**eqn. 4,9**). NC-Spz is also capable of inducing Toll endocytosis when binding it and thus contributing to signaling (**eqn. 9**), but signaling through NC-Spz happens at a much lower rate than C-Spz mediated signaling. **Eqns. 11-12** describe the induction of Dorsal nuclear localization by Toll signaling. **Eqn. 11** introduces the following constraint: the total amount of Dorsal (Nuclear- Dl_{in} and cytoplasmic- Dl_{out}) is constant and equals Dl_{tot} .

Full model equations

$$(\mathbf{1})\ \frac{\partial[W]}{\partial t} = D_W\nabla^2[W] - \alpha_w[W] + \beta(x)\frac{[Dl_{in}]^{n_W}}{K_W+[Dl_{in}]^{n_W}}$$

$$\beta(x) = \begin{cases} if\ \ x > X_{WntD} \rightarrow x \in wntD\ expression\ zone, & \beta_w \\ else, & 0 \end{cases}$$

$$(\mathbf{2})\ R_w = W_{lower} + (1 - W_{lower})\frac{W_{Tr}}{W_{Tr}+[W(x,t)]^{n_{lower}}}$$

$$(\mathbf{3})\ T_{tot} = [Tl] + [CSpz - Tl] + [NCSpz - Tl] + [Tl_{end}] \quad \rightarrow$$

$$[Tl] \ = T_{tot} - [CSpz - Tl] - [NCSpz - Tl] - [Tl_{end}]$$

$$(\mathbf{4})\ \frac{\partial[NCSpz]}{\partial t} = D_{NC}\nabla^2[NCSpz] - \alpha_{NC}[NCSpz] + \eta(x) - R_wK_{on}[Tl][NCSpz] + R_wK_{off}[NCSpz - Tl])$$

$$\eta(x) = \begin{cases} if\ x \in pipe\ domain, & \eta_0 \\ else, & 0 \end{cases}$$

$$(\mathbf{5})\ \frac{\partial[CSpz]}{\partial t} = -\alpha_C[CSpz] - R_wK_{on,c}[Tl][CSpz] + R_wK_{off,c}[CSpz - Tl] - K_{bind}[NSpz][CSpz] + K_{split}[NCSpz - Tl] + \frac{\lambda\eta(\vec{x})}{\eta_0}[NCSpz*]$$

$$(\mathbf{6})\ \frac{\partial[NSpz]}{\partial t} = D_{NC}\nabla^2[NSpz] - \alpha_{NC}[NSpz] - K_{bind}[NSpz][CSpz] + 2K_{split}[NCSpz - Tl]$$

$$(\mathbf{7})\ \frac{\partial[NCSpz*]}{\partial t} = D_{NC*}\nabla^2[NCSpz*] - \frac{\lambda\eta(\vec{x})}{\eta_0}[NCSpz*] + K_{bind}[NSpz][CSpz]$$

$$(\mathbf{8})\ \frac{\partial[CSpz - Tl]}{\partial t} = R_w[Tl][CSpz] - R_wK_{off,c}[CSpz - Tl] + K_{split}[NCSpz - Tl] - K_{end}[CSpz - Tl]$$

$$(\mathbf{9})\ \frac{\partial[NCSpz-Tl]}{\partial t} = R_wK_{on}[Tl][NCSpz] - (R_wK_{off} + K_{split} + K_{end})[NCSpz - Tl]$$

$$(\mathbf{10})\ \frac{\partial[Tl_{end}]}{\partial t} = K_{end}([CSpz - Tl] + [NCSpz - Tl]) - K_{rec}[Tl_{end}]$$

$$(\mathbf{11})[Dl_{Tot}] = [Dl_{in}] + [Dl_{out}]$$

$$(\mathbf{12})\frac{\partial[Dl_{in}]}{\partial t} = K_{Dl,in}[Tl_{end}][Dl_{out}] - K_{Dl,out}[Dl_{in}]$$

Full model parameter values selection

For most parameters, no biochemical measurements in the early embryo are available and biologically feasible values span several orders of magnitude. However, for some parameters restricting the realistic biochemical range is possible based on related measurements. We therefore base parameter values on the following considerations:

- **Length scale:** the circumference of the embryo is ~550 µm therefore the appropriate length for the ventral region where shuttling and feedback with WntD take place is 250 µm.
- **Diffusion rates:** the diffusion time of FITC-conjugated BSA in the peri-vitilline fluid was measured by D. Stein et. al. (Cell, 65 725- 735), who injected it into the peri-vitilline space of an embryo and observed equilibration time. They report uniform distribution within 10 minutes after the injection. BSA is a 66 kDa protein (larger than the 41 kDa WntD and 25 and 14 kDa N-Spz and C-Spz respectively). Taking into account the length of the embryo and assuming equilibration time corresponds to at least two diffusion times, we obtain an approximate range for the diffusion coefficients: 10^2 – 10^3 µm^2/ sec.
- **Receptor concentrations:** we assume that the surface facing the peri-vitilline space contains ~ 1000 receptors per nucleus. For a 10 µm^2 surface and a 0.5 µm wide peri-vitelline layer, receptor concentration is ~ 0.3µM.
- **Production rates:** we consider 50 molecules/nucleus/sec or 0.02 µM^−1/ sec as an upper bound on the range of production rates. In this study, we use lower values in the range of 1-3 molecules/nucleus/sec.
- **Degradation rates:** approximation for realistic values used in this study is based on measured Bicoid lifetime of 50-15 minutes during NC 12 to gastrulation respectively (Drocco et al. Biophys J. 2011). These values correspond to 0.0008-0.00024 1/sec.

For specific values consistent with the above and values for additional types of parameters, we used parameter ranges characterized in our previous publications as consistent with Self Organized Shuttling (SOSH) (Haskel-Ittah et al., 2012) and Induction-Contraction (InC) wntD based feedback (Rahimi et al., 2016). The SOSH WT parameters used in this work are the SOSH parameter values described in Table S5 of (Haskel-Ittah et al., 2012), with slight alterations to better resemble our experimental data. This parameter set belongs to the parameter sub space of “self-organized shuttling” as described in Table S3 of (Haskel-Ittah et al., 2012). In order to find this sub space of “self-organized shuttling”, Haskel-Ittah et al. conducted a thorough screen of parameter space, varying diffusion coefficients, reaction rates and protein concentrations over

several orders of magnitude. The parameter sub space exhibiting a sharp and robust Dl gradient was then selected. Haskel-Ittah et al. characterized the selected sub-space and showed it exhibits the following properties:

(1) no diffusion of the C-Spz
(2) N-Spz was degraded faster when in complex with C-Spz
(3) C-Spz and NC-Spz bind Tl weakly
(4) N-Spz diffuses slower than the NC-Spz* complex
(5) The dynamics of C-Spz interaction with Tl are faster than those of NC-Spz

Values for WntD related parameters (diffusion, degradation, and production rates) were based on our previous paper (Rahimi et al., 2016). The addition of Dorsal nuclear localization (eqns. 11-12) introduced new Dorsal-related parameters, which were selected to resemble similar parameters in the model (for example, the total concentration of Dorsal is similar to that of Toll). For the simulation of WntD mutants, model equations were solved with the WntD production rate set to zero.

Constant external gradient model

In order to simulate only Dorsal nuclear localization induced by a constant Toll signaling profile, the following set of equations was solved:

$$(\mathbf{13})\ \frac{\partial[Tl_{end}]}{\partial t} = 0, \qquad [Tl_{end}] = Tl_{end}^{final}(X)$$

$$(\mathbf{14})\ [Dl_{Tot}] = [Dl_{in}] + [Dl_{out}]$$

$$(\mathbf{15})\ \frac{\partial[Dl_{in}]}{\partial t} = K_{Dl,in}[Tl_{end}][Dl_{out}] - K_{Dl,out}[Dl_{in}]$$

The constant external gradient, Tl_{end}^{final}, was selected to be the sharp Toll signaling profile $[Tl_{end}]$ at the last time point for the simulation of the full model (eqns 1-12). Parameter values according to Table S1.

Naïve diffusion model

This model includes a single ligand, $NCSpz$, which is produced throughout the *pipe* domain (eqn. 17). The ligand diffuses and is degraded (eqn. 17). It binds the Toll receptor (eqns. 18,16), and induces Dorsal nuclear localization (eqns. 20-21). This model is described by the following equations:

$$(\mathbf{16})\ T_{tot} = [Tl] + [NCSpz - Tl] + [Tl_{end}] \rightarrow$$

$$[Tl] = T_{tot} - [NCSpz - Tl] - [Tl_{end}]$$

$$(\mathbf{17})\ \frac{\partial[NCSpz]}{\partial t} = D_{NC}\nabla^2[NCSpz] - \alpha_{NC}[NCSpz] + \eta(x) - K_{on}[Tl][NCSpz]$$

$+K_{off}[NCSpz - Tl])$

$$\eta(x) = \begin{cases} if\ x \in pipe\ domain, & \eta_0 \\ else, & 0 \end{cases}$$

$$(\mathbf{18})\ \frac{\partial[NCSpz-Tl]}{\partial t} = K_{on}[Tl][NCSpz] - (K_{off} + K_{end})[NCSpz - Tl]$$

$$(\mathbf{19})\ \frac{\partial[Tl_{end}]}{\partial t} = K_{end}([NCSpz - Tl]) - K_{rec}[Tl_{end}]$$

$$(\mathbf{20})[Dl_{Tot}] = [Dl_{in}] + [Dl_{out}]$$

$$(\mathbf{21})\ \frac{\partial[Dl_{in}]}{\partial t} = K_{Dl,in}[Tl_{end}][Dl_{out}] - K_{Dl,out}[Dl_{in}]$$

Parameter values according to Table S1. See further analytical and numerical analysis for the sharpness and robustness of the gradient in this model in (Haskel-Ittah et al., 2012).

The effects of shuttling parameters on double peak prominence

The prominence of the converging double peak feature in the shuttling model depends on model parameters which control the mean path that the shuttling complex travels ventrally before being cleaved, relative to the length of the source (the *pipe* domain). This mean path is influenced by several parameters, mainly tissue absolute length L (when maintaining the source as 40% of absolute length), changing source length directly by assuming the *pipe* domain is smaller or larger than 40% of the circumference, cleavage rate of the shuttling complex λ, and diffusion coefficient of the shuttling complex D_{NC*}. For a sufficiently large ratio between the mean path and L, no double peak will be observed. Lowering this ratio increases the prominence of the double peak. For a sufficiently small ratio, the double peak does not converge into a single peak, since the shuttling complex cannot penetrate all the way to the ventral most region. We demonstrate this by solving the full model for our WT parameter set (Table S1), and comparing to two sets where these parameters are perturbed (either decreased 2 fold or increased 2 fold).

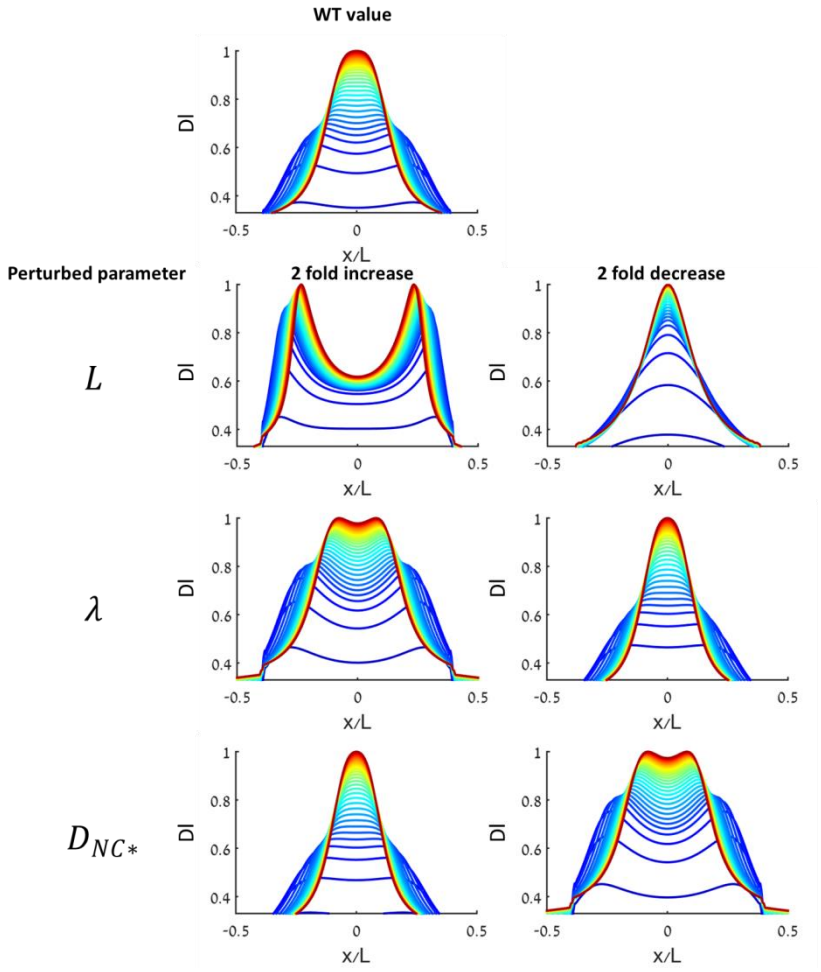

Model Supplement Figure 1 – Perturbations to shuttling complex parameters modulate double peak prominence.

References

Haskel-Ittah, M., Ben-Zvi, D., Branski-Arieli, M., Schejter, E. D., Shilo, B. Z. and Barkai, N. (2012). Self-organized shuttling: generating sharp dorsoventral polarity in the early Drosophila embryo. *Cell* **150**, 1016-1028.

Heemskerk, I. and Streichan, S. J. (2015). Tissue cartography: compressing bio-image data by dimensional reduction. *Nat Methods* **12**, 1139-1142.

Rahimi, N., Averbukh, I., Haskel-Ittah, M., Degani, N., Schejter, E. D., Barkai, N. and Shilo, B. Z. (2016). A WntD-Dependent Integral Feedback Loop Attenuates Variability in Drosophila Toll Signaling. *Dev Cell* **36**, 401-414.